Systematic study of the experimental measurements on J/ψ cross sections and kinematic distributions in p+p collisions at different energies

Wangmei Zha,[1,2] Bingchu Huang,[2] Rongrong Ma,[2] Lijuan Ruan,[2] Zebo Tang,[1,*] Zhangbu Xu,[2] Chi Yang,[1,2] Qian Yang,[1,2] and Shuai Yang[1,2]

[1]*Department of Modern Physics, University of Science and Technology of China, Hefei 230026, China*

[2]*Physics Department, Brookhaven National Laboratory, New York, New York 11973-5000, USA*

(Received 30 June 2015; revised manuscript received 29 December 2015; published 29 February 2016)

The world experimental data on cross section and kinematic distribution in $p + p$ and $p + A$ collisions at $\sqrt{s} = 6.8$–7000 GeV are systematically examined. The $\sqrt{s}$ dependence of the inclusive cross section, rapidity, and transverse momentum distributions are studied phenomenologically. We explore empirical formulas to obtain the total cross section, rapidity, and transverse momentum (p_T) distribution. This is crucial for the interpretation of $A + A$ J/ψ results at the BNL Relativistic Heavy Ion Collider when the $p + p$ reference data are not available. In addition, the cross section at midrapidity and transverse momentum distributions in $p + p$ collisions at $\sqrt{s} = 39$ and 62.4 GeV are evaluated.

DOI: 10.1103/PhysRevC.93.024919

I. INTRODUCTION

Lattice QCD predicts that, under conditions of extremely high temperatures and energy densities, a phase transition or crossover from hadronic matter to a new form of matter, known as quark gluon plasma (QGP) [1], will occur. The BNL Relativistic Heavy Ion Collider (RHIC) was built to search for the QGP and to study its properties in laboratory through high-energy heavy-ion collisions [2–5]. Many observables have been proposed to probe the QGP created in heavy-ion collisions. Among them, the J/ψ suppression caused by the color-charge screening in QGP is one of most important signatures [6].

Over the past 20 years, J/ψ production in hot and dense medium has been a topic attracting growing interest. Suppression of J/ψ production has been observed in various experimental measurements [7–10]. A similar suppression pattern and magnitude of J/ψ was observed at the CERN Super Proton Synchrotron (SPS) and RHIC despite more than one order of magnitude difference of collision energy. Furthermore, the J/ψ is suppressed more in forward rapidity than that in midrapidity at RHIC 200 GeV Au + Au collisions [11] and comparable J/ψ nuclear modifications have been observed by the PHENIX Collaboration at forward rapidity from $\sqrt{s_{NN}} = 39$ to 200 GeV in Au+Au collisions [12]. These experimental observations suggest that, in addition to color screening, there exist other effects contributing to the modification of J/ψ production. Cold nuclear matter (CNM) effects, the combined contribution of finite J/ψ formation time and finite space-time extent of QGP and recombination from uncorrelated c and $\bar{c}$ in the medium may account for these contributions [13]. Among these contributions, the regeneration of J/ψ from the recombination of $c\bar{c}$ plays an important role to explain the similar suppressions at SPS and RHIC. As the collision energy increases, the regeneration of J/ψ from the larger charm quark density would also increase which partly compensates for the additional suppression from color screening. The regeneration also expects a stronger suppression at forward rapidity at RHIC where the charm quark density is lower than that at midrapidity. At LHC, the J/ψ is less suppressed in both midrapidity and forward rapidity than that at RHIC [14,15], which may indicate that the regeneration contribution is dominant in the J/ψ production at CERN Large Hadron Collider (LHC) energies. Measurements of J/ψ in different collision energies at the Solenoidal Tracker at RHIC (STAR) can give us indications on the balance of these mechanisms for J/ψ production and medium properties.

To qualify the medium effects on the modification of J/ψ production, the knowledge of J/ψ cross section and kinematics in a $p + p$ collision is crucial to offer a reference. The hard interactions in $p + p$ collisions which create charm quark pairs are well calculated by perturbative QCD (pQCD). However, the subsequent soft process to form J/ψ hadron cannot be described within the framework of pQCD, which make it difficult to determine the cross section and kinematics of J/ψ precisely by model calculations. During RHIC year 2010, STAR has collected abundant events of Au + Au collisions at $\sqrt{s_{NN}} = 39$ and 62.4 GeV, while the reference data in $p + p$ collisions is not on the schedule of the RHIC run plan. There are several measurements from fixed target $p + A$ experiments [16–18] and Intersecting Storage Ring (ISR) collider experiments [19,20] at midrapidity near these two energy points. However, the p_T shapes from [19] and [20] at 63 GeV are inconsistent with each other and the cross section measurements at 39 GeV [16–18] are comparable to (or even larger than) that at 63 GeV [19,20]. Therefore, as what we did in Ref. [21], we study the world-wide data to obtain the J/ψ reference at these collision energies.

In this article, we report an interpolation of the p_T-integrated and differential inclusive J/ψ cross section in $p + p$ collisions at midrapidity to $\sqrt{s} = 39$ and 62.4 GeV. We establish a strategy to estimate the inclusive J/ψ cross section and kinematics at certain energy points, which makes

*zbtang@ustc.edu.cn

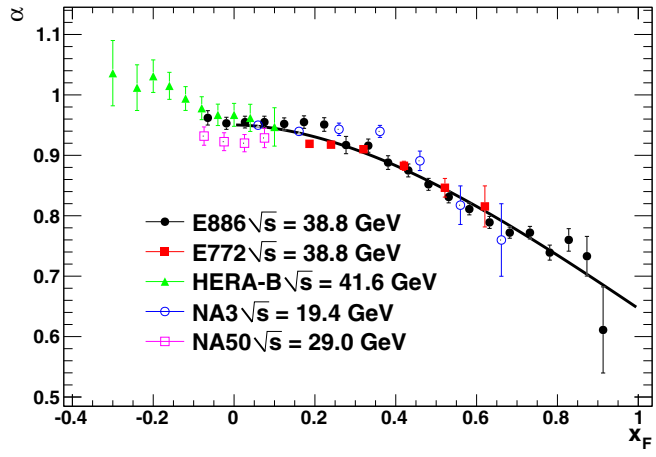

FIG. 1. Measurements of α defined in Eq. (1) as a function of x_F by various experiments in different collision energies [22–26]. The solid curve represents the parametrization of Eq. (2) discussed in the text.

the calculation of the J/ψ nuclear modification factors for any colliding system and energy at RHIC possible. The extrapolation is done in three steps:

(i) Energy interpolation of the existing total J/ψ cross section measurements.
(ii) Energy evolution of the rapidity distribution.
(iii) How transverse momentum distribution changes with energy.

II. AVAILABLE EXPERIMENTAL RESULTS TREATMENT

The measurements of J/ψ hadroproduction have been performed for about 40 years. In such a long period, different experimental techniques have been utilized and different input information was available at the time of the measurements. Therefore, a comparison of different experimental results on an equal footing needs an update of the published values on several common assumptions and aspects. For example, the branching ratio of $J/\psi \to e^+e^-$ (or $\mu^+\mu^-$) have changed with time; the assumed functional forms for the x_F and p_T shapes, which can be used to infer the total J/ψ production, are different in different measurements; and the treatment of the nuclear effects are not homogeneous. In this section, we update all the results with the current best knowledge of branching ratios, kinematics and nuclear effects.

The cross section for J/ψ on a nuclear target is often characterized by a power law:

$$\sigma^{pA}_{J/\psi} = \sigma^{pN}_{J/\psi} \times A^{\alpha}, \tag{1}$$

where $\sigma^{pA}_{J/\psi}$ is the corresponding proton-nucleus cross section for a target of atomic mass number A, $\sigma^{pN}_{J/\psi}$ is the J/ψ proton-nucleon cross section, and α is the parameter which characterizes the nuclear dependence.

The dependences of α on x_F measured by NA3 [22], NA50 [23], E772 [24], E886 [25], and HERA-B [26] are shown in Fig. 1, where x_F is defined as $x_F = 2p_z/\sqrt{s}$(p_z is longitudinal momentum, along the beam direction.). No significant energy dependence of α as a function of x_F is observed within uncertainties, thus we assume it is independent of the cms energy ($\sqrt{s}$). The results of $J/\psi\alpha$ at $x_F > 0$ can be represented for convenience by simple parametrization shown as solid line in Fig. 1:

$$\alpha(x_F) = a \times e^{-\ln 2(\frac{x_F}{b})^c}, \tag{2}$$

where $a = 0.950 \pm 0.003$, $b = 1.38 \pm 0.05$, and $c = 1.81 \pm 0.09$. The J/ψ cross section in proton nucleon collisions is extracted from nuclear target experiments using Eq. (1), wherein the parameter α are interpolated from the data shown in Fig. 1 with Eq. (2). Some of the experimental measurements are only quoted for a limited phase-space. To obtain the total cross sections, the functional forms of x_F and p_T spectrum shapes [26] utilized for extrapolation are

$$\frac{d\sigma}{dx_F} = a \times e^{-\ln 2(\frac{x_F}{b})^c}, \tag{3}$$

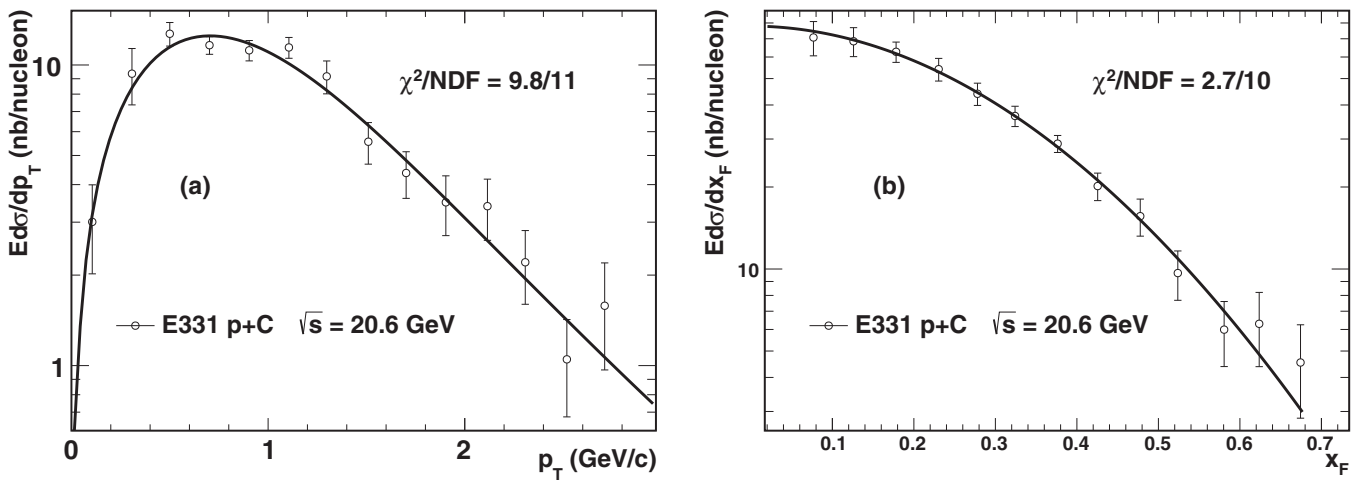

FIG. 2. Distributions of (a) $Ed\sigma/dp_T$ and (b) $Ed\sigma/dx_F$ in $p + C$ collisions at $\sqrt{s} = 20.6$ GeV measured by E331 collaboration [32]. The solid lines are fit curves with the functional forms described in the text.

$$\frac{d\sigma}{dp_T} = d \times \frac{p_T}{\left(1 + e^2 p_T^2\right)^f}, \tag{4}$$

respectively, where a, b, c, d, e, and f are free parameters. As illustrated in Fig. 2, these two functional forms describe the x_F and p_T spectra very well. All the measurements are updated with the latest branching fractions ($5.961 \pm 0.032\%$ for $J/\psi \to \mu^+ + \mu^-$, $5.971 \pm 0.032\%$ for $J/\psi \to e^+ + e^-$) [27]. The treated results on J/ψ cross sections [16–18,22,23,28–39,41–44,48] are listed in Table I. They show a good overall consistency, even though some of them contradict with each other. For example, the two measurements (E331 [32] and E444 [33]) at 20.6 GeV deviate from each other by roughly 2σ; the E705 measurement [34] at 23.8 GeV is higher than the UA6 [35] one at 24.3 GeV by more than 2σ. There are no reports on global systematic uncertainties in these experiments which could cover the differences.

III. RESULTS

The energy evolution of the total inclusive J/ψ production cross section in proton induced interactions is shown in Fig. 3. The first approach is to use the predicted shape in the color evaporation model (CEM) at next to leading order (NLO) [45] to describe the energy dependence of the J/ψ cross section. The central CT10 parton density set [46] and $\{m, \mu_F/m, \mu_R/m\} = \{1.27\,(\text{GeV}), 2.10, 1.60\}$ set is utilized in the predicted shape, where m is the charm quark mass, μ_F is the factorization scale, μ_R is the renormalization scale. The fit is defined such that the normalization of the NLO CEM calculation is left as a free parameter (α): $\sigma = \alpha \times \sigma_{\text{CEM}}$. The

TABLE I. Updated total ($\sigma_{J/\psi}$) production cross sections in proton-induced interactions.

Experiment	Reaction	$\sqrt{s}$ (GeV)	$\sigma_{J/\psi}$ (nb/nucleon)
CERN-PS [28]	$p + A$	6.8	0.732 ± 0.13
WA39 [29]	$p + p$	8.7	2.35 ± 1.18
IHEP [30]	p + Be	11.5	21.63 ± 5.64
E331 [31]	p + Be	16.8	85.15 ± 21.30
NA3 [22]	p + Pt	16.8	95.0 ± 17.0
NA3 [22]	p + Pt	19.4	122.6 ± 21
NA3 [22]	$p + p$	19.4	120 ± 22
E331 [32]	p + C	20.6	278 ± 32.8
E444 [33]	p + C	20.6	176.5 ± 23.3
E705 [34]	p + Li	23.8	271.51 ± 29.84
UA6 [35]	$p + p$	24.3	171.42 ± 22.21
E288 [36]	p + Be	27.4	294.12 ± 73.53
E595 [37]	p + Fe	27.4	264 ± 56
NA38/51 [38,39]	$p + A$	29.1	229.5 ± 34.4
NA50 [23]	$p + A$	29.1	250.7 ± 37.6
E672/706 [18]	pBe	31.6	343.07 ± 75.12
E771 [16]	p + Si	38.8	359.1 ± 34.2
E789 [17]	p + Au	38.8	415.04 ± 100
ISR [48]	$p + p$	52	716 ± 303
PHENIX [41]	$p + p$	200	3032 ± 288
CDF [42]	$p + \bar{p}$	1960	22560 ± 3384
ALICE [43]	$p + p$	2760	29912.6 ± 5384.3
ALICE [44]	$p + p$	7000	54449.4 ± 8494

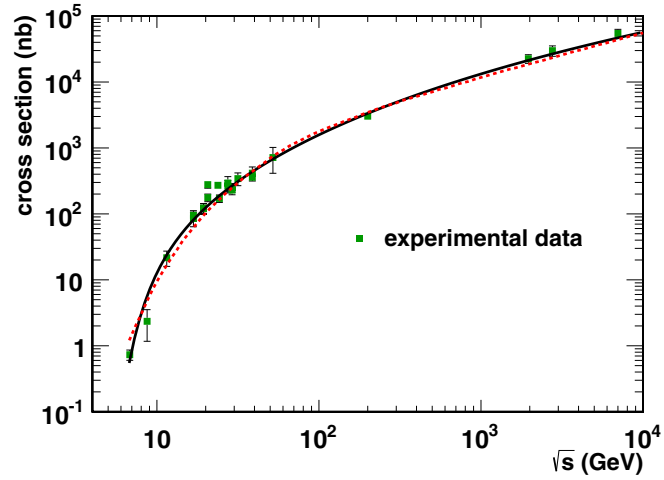

FIG. 3. Energy dependence of inclusive J/ψ production cross section [16–18,22,23,28–39,41–44,48]. The dashed line is the fit from CEM shape [45]. The solid line is a function fit of Eq. (5) as discuss in the text.

second approach is to use a functional form to describe the cross section energy evolution:

$$f(\sqrt{s}) = a \times y_{\text{max}}^d \times e^{\frac{-b}{y_{\text{max}}^c}}, \tag{5}$$

where $y_{\text{max}} = \ln(\frac{\sqrt{s}}{m_{J/\psi}})$ is the beam rapidity; a, b, c, and d are free parameters. As shown in Fig. 3, both approaches can describe the energy evolution trend of the J/ψ cross section. The χ^2/NDF for CEM and Eq. (5) fit are 92.9/22 and 52.6/19, respectively. The large χ^2 mainly comes from three experimental points which contradict with the common trend (E331 and E444 measurements at 20.6 GeV, E705 measurement at 23.8 GeV). If we exclude these three data points and refit the results, the χ^2/NDF for CEM and Eq. (5) fit are 41.6/19 and 15.5/16, respectively. The values extrapolated (without the three experimental points which deviate from the common trend most) for the J/ψ cross sections at $\sqrt{s} = 39$ and 62.4 GeV, utilizing the Eq. (5) and the NLO CEM based fit are listed in Table II. The result from NLO CEM based fit has been adopted as default set, the difference between these two fits has been quoted as systematic uncertainty.

The knowledge of the rapidity dependence of J/ψ production at different cms energies is crucial to obtain a reference for the measurements at midrapidity from RHIC. Based on a universal energy scaling behavior in the rapidity

TABLE II. Extrapolated values of the J/ψ production cross section at $\sqrt{s} = 39$ and 62.4 GeV. The difference between CEM and function fit has been taken as the systematic uncertainties of the extrapolation.

Fit	Cross section (nb/nucleon)	
	$\sqrt{s} = 39$ GeV	$\sqrt{s} = 62.4$ GeV
NLO CEM	416±16	924±36
Eq. (5)	407±19	828±39
evaluated results	416±16±9	924±36±96

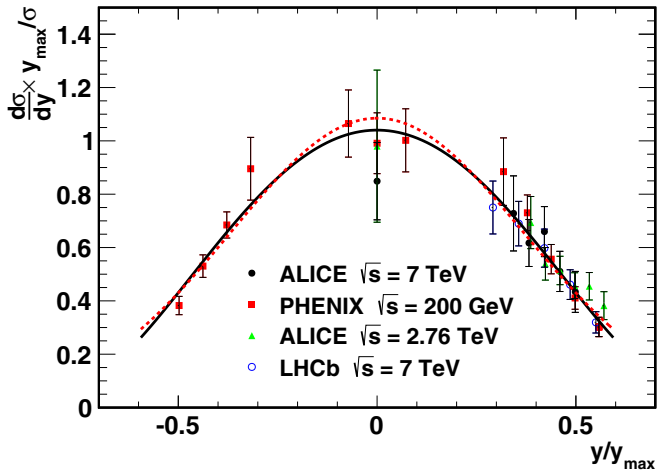

FIG. 4. Normalized J/ψ production cross section as a function of $y/y_{\rm max}$. The solid line and the dashed line are the function fit of Eqs. (6) and (7), respectively. The difference between these two fits has been considered as systematic errors.

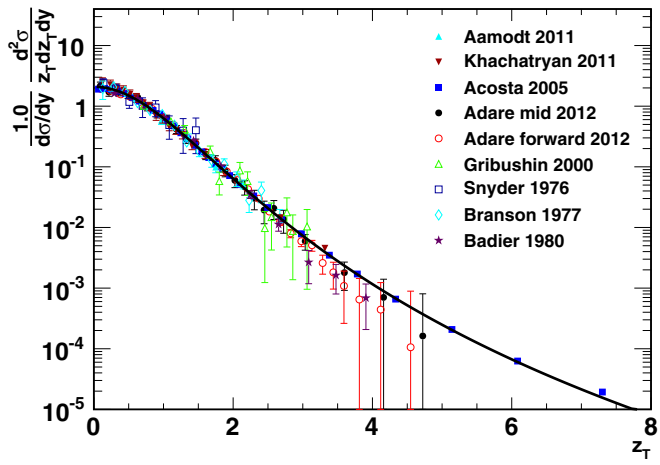

FIG. 5. J/ψ z_T distributions for available experimental results from $\sqrt{s} = 10$ to 7000 GeV. The solid line is a function fit as discussed in the text. The experimental data are from ALICE (Aamodt 2011: [44]), CMS (Khachatryan 2011: [49]), CDF (Acosta 2005: [42]), PHENIX (Adare mid 2012: [41] and Adare forward 2012: [41]), E672 & E706(Gribushin 2000: [18]), E288 (Snyder 1976: [36]), E331 (Branson 1977: [32]), and NA3 (Badier 1980: [22]) experiments.

$(y = \frac{1}{2}\ln\frac{E+p_z}{E-p_z})$ distribution obtained at different cms energies, we explore approaches to the extrapolation of the rapidity distribution. As shown in Fig. 4, the y-differential cross sections at different cms energies have been normalized by the total cross section $\sigma_{J/\psi}$, and the normalized values are plotted verse $y/y_{\rm max}$, where $y_{\rm max}$ has been previously defined. Despite more than one order of magnitude difference of collision energy, the treated RHIC [41] and LHC [43,44,47] experimental distributions fall into a universal trend, which allows us to perform global fits to all the experimental results with suitable functions. Two functional forms are chosen to describe the normalized $d\sigma/dy$:

$$\frac{1}{\sigma}\frac{d\sigma}{d(y/y_{\rm max})} = ae^{-\frac{1}{2}(\frac{y/y_{\rm max}}{b})^2}, \tag{6}$$

$$\frac{1}{\sigma}\frac{d\sigma}{d(y/y_{\rm max})} = \frac{c}{1-(y/y_{\rm max})^2}e^{-d(\ln(\frac{1+y/y_{\rm max}}{1-y/y_{\rm max}}))^2}, \tag{7}$$

where a, b, c, and d are free parameters. Both of them can describe the global distribution very well [$\chi^2/{\rm NDF} = 10.1/27$ for Eq. (6), $\chi^2/{\rm NDF} = 11.2/27$ for Eq. (7)]. The fit of Eq. (6) has been taken as a default set. The difference between these two fits has been considered as systematic uncertainties. With the extrapolated J/ψ cross sections and rapidity distributions, the predicted J/ψ cross section times branching ratio at $\sqrt{s} = 39$ and 62.4 GeV at midrapidity are $Br(e^+e^-)d\sigma/dy|_{|y|<1.0} = 8.97 \pm 0.59$ and 17.64 ± 2.12 nb, respectively. The uncertainties are the quadratic sum of statistical and systematic uncertainties from both total cross section and rapidity distribution estimations. These values are consistent with the estimations from CEM model (8.7 ± 4.5 nb for 39 GeV, 17.4 ± 8.0 for 62.4 GeV).

The energy evolution of J/ψ transverse momentum distribution is also studied via available experimental measurements from $\sqrt{s} = 10$–7000 GeV [18,19,22,32,34,36,41,42,44,49]. We used light target data (p [22], Be [18,36], Li [34], and C [32]) to minimize cold nuclear matter effects. In order to compare the different experimental measurements at different energies and rapidity domains, as shown in Fig. 5, the transverse momentum distributions are normalized by their p_T-integrated cross sections and plotted versus the z_T variable, which is defined as $z_T = p_T/\langle p_T\rangle$. The treated distributions follow a universal trend despite of the different cms energies and rapidity domains. We can describe the global distributions very well by the following function:

$$\frac{1}{d\sigma/dy}\frac{d^2\sigma}{z_T dz_T dy} = a \times \frac{1}{\left(1+b^2 z_T^2\right)^n}, \tag{8}$$

where $a = 2b^2(n-1), b = \Gamma(3/2)\Gamma(n-3/2)/\Gamma(n-1)$, and n is the only free parameter. From the fit, we obtain $n = 3.94 \pm 0.03$ with $\chi^2/{\rm NDF} = 105.9/151$.

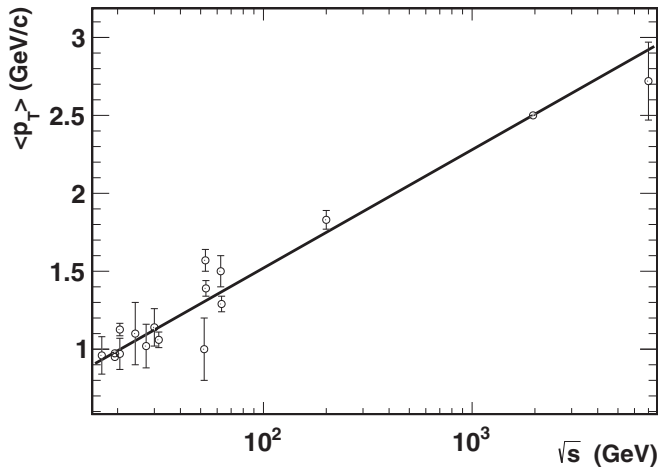

FIG. 6. J/ψ $\langle p_T\rangle$ at midrapidity as a function of cms energy from $\sqrt{s} = 10$ to 7000 GeV. The solid line is a fit of Eq. (9) to the data as discussed in the text.

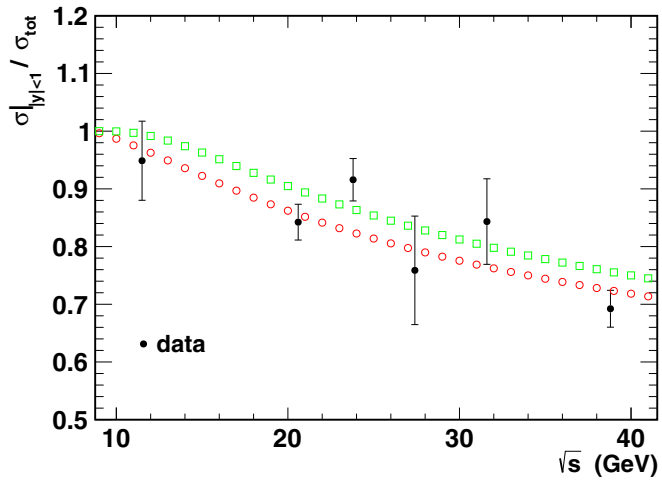

FIG. 7. The ratios of J/ψ $\sigma|_{|y|<1.0}$ to $\sigma_{\rm tot}$ as a function of cms energy [16–18,30,32–34,37,50]. The open circle and the open square are the estimations using the function fit of Eqs. (6) and (7) in Fig. 4, respectively.

With the universal shape and $\langle p_T \rangle$ information at certain energy and rapidity domain (we focus on midrapidity) we can extrapolate the transverse momentum distribution at any cms energy. Thus the next step is to evaluate the energy evolution of $\langle p_T \rangle$. The $\langle p_T \rangle$ at midrapidity as a function of cms energy from world-wide experiments [18,19,22,32,36,40–42,44,48] is shown in Fig. 6. Again, only part of the world-wide fixed-target data (with p, Be, Li, and C, respectively) are used to reduce the cold nuclear matter effects. The $\langle p_T \rangle$ versus energy can be fitted by the function form:

$$f(\sqrt{s}) = p + q \ln \sqrt{s}, \tag{9}$$

where p, q are free parameters. The fit parameters are $p = 0.0023 \pm 0.0182$, $q = 0.329 \pm 0.031$ with $\chi^2/\mathrm{NDF} = 41.1/15$. The estimated $\langle p_T \rangle$ from the fit function at $\sqrt{s} = 39$ and 62.4 GeV are 1.21 ± 0.04 and 1.36 ± 0.04 GeV/c, respectively. With these inputs, the transverse momentum distribution at these two cms energies can be completely determined.

TABLE III. The interpolations of cross section and p_T distribution at $\sqrt{s} = 39$ and 62.4 GeV.

Rapidity range	Cross section (nb/nucleon)	
$\lvert y\rvert < \infty$	$\sqrt{s} = 39$ GeV	$\sqrt{s} = 62.4$ GeV
$\lvert y\rvert < 1$	416 ± 18	924 ± 103
	301 ± 20	592 ± 71
Parameters of Eq. (8)	p_T distribution	
	$\sqrt{s} = 39$ GeV	$\sqrt{s} = 62.4$ GeV
n	3.94 ± 0.03	3.94 ± 0.03
$\langle p_T \rangle$	1.21 ± 0.04	1.36 ± 0.04

Lastly, one needs to determine the portion of the total cross section at midrapidity. There are rare rapidity distribution measurements in $p + A$ collisions at $\sqrt{s} < 200$ GeV. Therefore, the universal energy scaling parameters of rapidity distributions are determined by the measurements at $\sqrt{s} \geqslant 200$ GeV. Its validity at low-energy (<200 GeV) range still needs to be further investigated, but we do have various x_F distribution measurements of J/ψ in fixed-target experiments [16–18,30,32–34,37,50]. Together with the α verse x_F curve in Fig. 1 and the transverse momentum distributions obtained using the strategy described above, we can evaluate the rapidity distributions via the x_F distributions measurements in the fix-target experiments to check the validity of the rapidity interpolation method. The ratios of J/ψ $\sigma|_{|y|<1.0}$ to $\sigma_{\rm tot}$, which are calculated utilizing the evaluated rapidity distributions in fix-target experiments, versus cms energy are shown in Fig. 7. The two sets of open points plotted in the figure are obtained as follows:

(i) Parametrize the universal $\frac{1}{\sigma}\frac{d\sigma}{d(y/y_{\rm max})}$ versus $y/y_{\rm max}$ trend in Fig. 4 by Eqs. (6) and (7), respectively.
(ii) Extract the rapidity distribution ($\frac{1}{\sigma}\frac{d\sigma}{dy}$ versus y) utilizing the parametrizations of Eqs. (6) and (7), respectively.

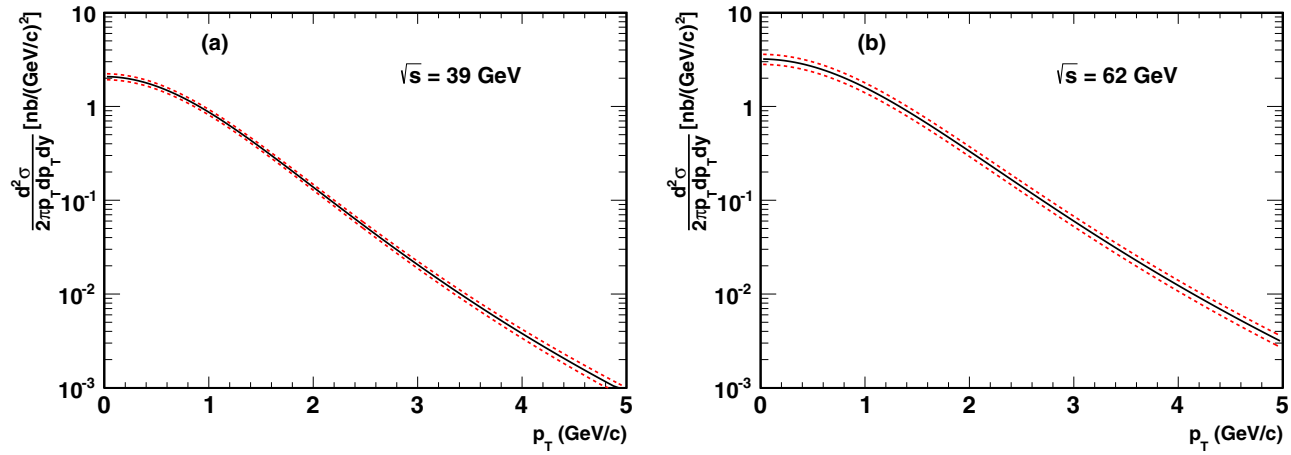

FIG. 8. The expected J/ψ differential cross section versus p_T at midrapidity ($|y| < 1$) for (a) 39 and (b) 62 GeV, respectively. The dashed lines represent for the uncertainties from interpolation.

(iii) Calculate the ratios of J/ψ $\sigma|_{|y|<1.0}$ to σ_{total} according the rapidity distributions at certain energies.

In this figure, we can see that our extrapolation strategy also works at low cms-energy range.

Finally, the interpolations of the p_T-integrated and differential inclusive J/ψ cross section in $p+p$ collisions at midrapidity could be accomplished as follows:

(1) The total cross section of J/ψ at certain energy could be extracted through the curves shown in Fig. 3.
(2) The shape of the rapidity distribution at certain energy could be derived from the universal trend depicted in Fig. 4. The cross section at midrapidity can be evaluated in conjunction with the total cross section.
(3) The p_T distribution at certain energy in midrapidity could be obtained via the parametrization of Eq. (8) illustrated in Fig. 5 with $\langle p_T \rangle$ extracted from Fig. 6. Together with the cross section at midrapidity, the p_T differential cross section at midrapidity is done.

The interpolations at $\sqrt{s} = 39$ and 62.4 GeV are listed in Table III and shown in Fig. 8.

IV. SUMMARY

We study the world-wide data of J/ψ production and kinematics at $\sqrt{s} = 6.8$–7000 GeV. We have developed a strategy to interpolate the J/ψ cross section, rapidity distribution, and transverse momentum distribution at any cms energy in $\sqrt{s} = 6.8$–7000 GeV. The rapidity and transverse momentum distributions measured in different energies have a universal energy scaling behavior. With this strategy, we predicted that the J/ψ cross section times branching ratio at $\sqrt{s} = 39$ and 62.4 GeV in midrapidity are $Br(e^+e^-)d\sigma/dy|_{|y|<1.0} = 8.97 \pm 0.59$, 17.64 ± 2.12 nb, respectively.

ACKNOWLEDGMENTS

We express our gratitude to the STAR Collaboration and the RCF at BNL for their support. The authors from USTC are supported by MOST under Grant No. 2014CB845400, the National Natural Science Foundation of China under Grant Nos. 11375172 and 11505180, China Postdoctoral Science Foundation funded project, and the Fundamental Research Funds for the Central Universities. The authors from BNL are supported by the U.S. DOE Office of Science under Contract No. DE-SC0012704.

[1] P. Braun-Munzinger and J. Stachel, Nature **448**, 302 (2007).
[2] I. Arsene *et al.* (BRAHMS Collaboration), Nucl. Phys. A **757**, 1 (2005).
[3] K. Adcox *et al.* (PHENIX Collaboration), Nucl. Phys. A **757**, 184 (2005).
[4] B. B. Back *et al.* (PHOBOS Collaboration), Nucl. Phys. A **757**, 28 (2005).
[5] J. Adams *et al.* (STAR Collaboration), Nucl. Phys. A **757**, 102 (2005).
[6] T. Matsui and H. Satz, Phys. Lett. B **178**, 416 (1986).
[7] M. C. Abreu *et al.*, Phys. Lett. B **477**, 28 (2000).
[8] B. Alessandro *et al.*, Eur. Phys. J. C **39**, 335 (2005).
[9] B. Alessandro *et al.*, Eur. Phys. J. C **48**, 329 (2006).
[10] A. Adare *et al.*, Phys. Rev. Lett. **98**, 232301 (2007).
[11] A. Adare *et al.*, Phys. Rev. C **84**, 054912 (2011).
[12] A. Adare *et al.*, Phys. Rev. C **86**, 064901 (2012).
[13] F. Karsch *et al.*, Phys. Lett. B **193**, 105 (1987).
[14] B. Abelev *et al.*, Phys. Rev. Lett. **109**, 072301 (2012).
[15] B. Abelev *et al.*, Phys. Lett. B **734**, 314 (2014).
[16] T. Alexopoulos *et al.*, Phys. Rev. D **55**, 3927 (1997).
[17] M. H. Schub *et al.*, Phys. Rev. D **52**, 1307 (1995).
[18] A. Gribushin *et al.*, Phys. Rev. D **62**, 012001 (2000).
[19] A. G. Clark *et al.*, Nucl. Phys. B **142**, 29 (1978).
[20] C. Kourkounelis *et al.*, Phys. Lett. B **91**, 481 (1980).
[21] W. Zha, C. Yang, B. Huang, L. Ruan, S. Yang, Z. Tang, and Z. Xu, Phys. Rev. C **88**, 067901 (2013).
[22] J. Badier *et al.*, Z. Phys. C **20**, 101 (1983).
[23] B. Alessandro *et al.* (NA50 Collaboration), Eur. Phys. J. C **33**, 31 (2004).
[24] D. M. Alde, H. W. Baer, T. A. Carey, G. T. Garvey, A. Klein, C. Lee, M. J. Leitch, J. Lillberg, P. L. McGaughey, C. S. Mishra, J. M. Moss, J. C. Peng, C. N. Brown, W. E. Cooper, Y. B. Hsiung, M. R. Adams, R. Guo, D. M. Kaplan, R. L. McCarthy, G. Danner, M. Wang, M. Barlett, and G. Hoffmann, Phys. Rev. Lett. **66**, 133 (1991).
[25] M. J. Leitch *et al.* (FNAL E866/NuSea Collaboration) Phys. Rev. Lett. **84**, 3256 (2000).
[26] I. Abt *et al.*, Eur. Phys. J. C **60**, 525 (2009).
[27] K. A. Olive *et al.*, Chin. Phys. C **38**, 090001 (2014).
[28] A. Bamberger *et al.*, Nucl. Phys. B **134**, 1 (1978).
[29] M. J. Corden *et al.*, Phys. Lett. B **98**, 220 (1981).
[30] Yu. M. Antipov *et al.*, Phys. Lett. B **60**, 309 (1976).
[31] K. J. Anderson *et al.*, Phys. Rev. Lett. **36**, 237 (1976).
[32] J. G. Branson, G. H. Sanders, A. J. S. Smith, J. J. Thaler, K. J. Anderson, G. G. Henry, K. T. McDonald, J. E. Pilcher, and E. I. Rosenberg, Phys. Rev. Lett. **38**, 1331 (1977).
[33] K. J. Anderson, R. N. Coleman, G. E. Hogan, K. P. Karhi, K. T. McDonald, C. B. Newman, J. E. Pilcher, E. I. Rosenberg, G. H. Sanders, A. J. S. Smith, and J. J. Thaler, Phys. Rev. Lett. **42**, 944 (1979).
[34] L. Antoniazzi *et al.*, Phys. Rev. D **46**, 4828 (1992).
[35] C. Morel *et al.*, Phys. Lett. B **252**, 505 (1990).
[36] H. D. Snyder *et al.*, Phys. Rev. Lett. **36**, 1415 (1976).
[37] E. J. Siskind, B. C. Barish, J. F. Bartlett, A. Bodek, K. W. B. Merritt, M. H. Shaevitz, A. M. Diamant-Berger, J. P. Dishaw, M. Faessler, J. K. Liu, F. S. Merritt, and S. G. Wojcicki, Phys. Rev. D **21**, 628 (1980).
[38] M. C. Abreu *et al.*, Phys. Lett. B **444**, 516 (1998).
[39] M. C. Abreu *et al.*, Phys. Lett. B **438**, 35 (1998).
[40] E. Nagy *et al.*, Phys. Lett. B **60**, 96 (1975).
[41] A. Adare *et al.* (PHENIX Collaboration), Phys. Rev. D **85**, 092004 (2012).
[42] D. Acosta *et al.* (CDF Collaboration), Phys. Rev. D **71**, 032001 (2005).
[43] B. Abelev *et al.* (ALICE Collaboration), Phys. Lett. B **718**, 295 (2012).

[44] K. Aamodt *et al.* (ALICE Collaboration), Phys. Lett. B **704**, 442 (2011).
[45] R. E. Nelson, R. Vogt, and A. D. Frawley, Phys. Rev. C **87**, 014908 (2013).
[46] H.-L. Lai, M. Guzzi, J. Huston, Z. Li, P. M. Nadolsky, J. Pumplin, and C.-P. Yuan, Phys. Rev. D **82**, 074024 (2010).
[47] R. Aaij *et al.* (LHCb Collaboration), Eur. Phys. J. C **71**, 1645 (2011).
[48] E. Amaldi *et al.*, Lettere al Nuovo Cimento **19**, 152 (1977).
[49] V. Khachatryan *et al.* (CMS Collaboration), Eur. Phys. J. C **71**, 1575 (2011).
[50] M. S. Kowitt *et al.*, Phys. Rev. Lett. **72**, 1318 (1994).